INORGANIC CHEMISTRY FRONTIERS

RESEARCH ARTICLE

View Article Online
View Journal | View Issue

Cite this: *Inorg. Chem. Front.*, 2024, **11**, 3984

Anti-Kasha's rule in phenothiazine derivatives and metal–organic frameworks: mechanism investigation and application in hypochlorite detection†

Tingting Wu,[a] Mingyuan Lei,[a,b] Fayuan Ge,[a] Yang Liu,[a] Minqi Xia,[c] Lijun Yang [c] and Hegen Zheng *[a]

Received 3rd April 2024,
Accepted 16th May 2024

DOI: 10.1039/d4qi00838c

rsc.li/frontiers-inorganic

In recent years, some organic molecules have been found to produce luminescence that does not obey Kasha's rule in the aggregate state. This luminescence often originates from upper and the lowest energy-excited states. However, developing more single-component compounds with anti-Kasha's rule emissions and expanding their applications remains challenging. Herein, two phenothiazine derivatives are found to have anti-Kasha's rule luminescence in the aggregate state. Studies on photophysical properties, single-crystal structures, femtosecond transient absorption (fs-TA), and theoretical calculations indicate that the restriction of intramolecular motions (RIM) is the mechanism for the multiwavelength emission. Furthermore, a new luminescent Cd MOF, **Cd-PTZ-db**, which inherits the luminescence and structural characteristics of the phenothiazine derivative ligand, demonstrates great potential in the detection of hypochlorite (ClO^-). This work gains a deeper understanding of the effect of RIM on luminescence in the aggregated state, and once again proves that the rigid structures of MOFs can work as the foundation for developing advanced solid-state emissive materials and other practical applications.

1 Introduction

Most luminogens obey Kasha's rule, according to which luminogens typically emit from the lowest excited state, independent of the excitation energy.[1] In contrast, some cases (*e.g.*, azulenes,[2–4] and triazine[5]) produce anomalous emission from higher excited states in very dilute solutions, because of their ultrafast radiative rate or large S_2–S_1 energy gap. These so-called anti-Kasha's rule emissions are of great theoretical and experimental importance as they avoid the additional consumption associated with internal transitions and other types of electronic internal conversion (IC) processes, thus increasing the fluorescence quantum efficiency.[6] However, these anti-Kasha's rule emissions are often difficult to see in neat solids because the high concentrations of molecules in the solid-state keep the higher excited states of molecules vibrational and collisionally equilibrated, preventing emission from upper excited states. Recently, several single-component luminogens were reported to exhibit anti-Kasha's rule emissions in solid and crystalline states, including luminescent metal–organic frameworks (MOFs),[7] but underlying mechanisms are still a subject of debate. Some studies suggest that the reason for solid materials exhibiting anti-Kasha's rule emission, which may be similar to aggregation-induced emission (AIE), is the restriction of intramolecular motions (RIM).[8,9] RIM reduces non-radiative transitions and suppresses IC of these compounds. Given that the rigid structures of MOFs can restrict the molecular motion through coordination bonds between ligands and metals[10] and make them promising in AIE,[11,12] MOFs also have the potential for solid-state anti-Kasha's rule emission.

MOFs, as an emerging class of highly crystalline materials, exhibit wide applications including in gas storage and separation and catalysis, etc.[13–19] MOFs also distinguish themselves as a promising luminescent material,[20–24] offering precise control over their luminescence characteristics through tailored ligand and metal ion designs, setting them apart from organic luminescent materials. Furthermore, the abundance

[a]*State Key Laboratory of Coordination Chemistry, School of Chemistry and Chemical Engineering, Collaborative Innovation Center of Advanced Microstructures, Nanjing University, Nanjing 210023, Jiangsu, P. R. China. E-mail: zhenghg@nju.edu.cn*
[b]*Key Laboratory of Evidence Identification in Universities of Shandong Province, Shandong University of Political Science and Law, Jinan, Shandong 250014, P R China*
[c]*Key Laboratory of Mesoscopic Chemistry of MOE and Jiangsu Provincial Laboratory for Nanotechnology, School of Chemistry and Chemical Engineering, Nanjing University, Nanjing 210023, Jiangsu, P R China*

†Electronic supplementary information (ESI) available. CCDC 2303468 and 2303469. For ESI and crystallographic data in CIF or other electronic format see DOI: https://doi.org/10.1039/d4qi00838c

of reactive sites on the ligands and metal ions makes MOFs widely applicable in the field of luminescence detection.[25–29]

In this work, we have modified phenothiazine with two methyl benzoate or benzoic acids, to form dimethyl 4,4′-(10*H*-phenothiazine-3,7-diyl)dibenzoate (**PTZ-dbo**) and 4,4′-(10*H*-phenothiazine-3,7-diyl)dibenzoic acid (H_2PTZ-dba). **PTZ-dbo** exhibits anti-Kasha's rule emissions in the water suspension and the solid state that are different from that in the isolated state in tetrahydrofuran (THF) solution. Further analysis of the single crystal structures, photophysical studies, femtosecond transient absorption (fs-TA) spectroscopies, and theoretical calculations indicate that large energy gaps between the two excited states of molecules in the aggregated state under RIM allow them to emit from upper excited singlet states. Furthermore, a new luminescent Cd-MOF, $\{[Cd(PTZ\text{-}dba)]\cdot 2H_2O\}_n$ (**Cd-PTZ-db**), is obtained by treating H_2PTZ-dba with Cd^{2+} ions. **Cd-PTZ-db** inherits the anti-Kasha's rule emission and as shown in Scheme 1, **Cd-PTZ-db** is able to withstand hypochlorite (ClO^-) oxidation. Its emission is not only retained but also enhanced after the oxidation. Remarkably, **Cd-PTZ-db** achieves a rapid, on-demand detection of ClO^- in aqueous solution, with a low limit of detection of 26 nM. In addition, **Cd-PTZ-db**-based strips have been successfully prepared to meet the need for the convenient detection of ClO^- in aqueous environments. In this way, this work provides a new perspective that RIM can also suppress Kasha's rule, leading to multi-coloured emission from the lowest and upper excited states of a single-component compound in the aggregated state.

2 Results and discussion

2.1 Photophysical characteristics

Derivatives of phenothiazine are classic luminogens, and the derivative we synthesized, **PTZ-dbo**, also exhibits strong fluorescence in THF solution. The steady-state emission spectra of **PTZ-dbo** were investigated initially. As shown in Fig. 1a, **PTZ-dbo** exhibits the characteristic aggregation-caused quenching phenomenon, demonstrating bright luminescence in organic solvents, but dimmed emission in aqueous suspensions. Interestingly, as shown in Fig. 1b, as the proportion of water increases, a short-wavelength emission at around 410 nm is revealed, which differs from its behavior in THF solution. To study the new emission, the excitation-wavelength-dependent steady-state emission spectra of **PTZ-dbo** in the water suspension were investigated (Fig. 1c). Under excitation at 352 nm, dual emissions consisting of short- and a long-wavelength emissions are clearly visible, with maximum wavelengths of 410 nm and 516 nm, respectively. The relative strength of two emission bands is strongly dependent on the excitation wavelength, with higher energy excitations resulting in enhanced emissions at shorter wavelengths. Additionally, in the aqueous environment, the lifetime of the 410 nm emission is 8 ns, which is different from the 0.4 ns of the 516 nm emission (Fig. S1†). These results strongly indicate that the dual emissions of **PTZ-dbo** in a water suspension emanate from more than one excited state. Similar behavior was observed with H_2PTZ-dba. In dilute THF solutions, H_2PTZ-dba emits a bright green luminescence at 525 nm, whereas in environments with water, a faint emission at 424 nm appears (Fig. S2†).

The UV-vis absorption was measured to determine whether any intermolecular interactions or molecular changes appear in the aggregated state. As shown in Fig. S3,† **PTZ-dbo** in the solid-state maintains similar UV-vis absorption peaks to those suspended in water and in THF solutions. The single-crystal X-ray diffraction (SCXRD) analysis shows that **PTZ-dbo** crystallizes in the orthogonal space group $Cmc2_1$ and consists of half a **PTZ-dbo** ligand in the asymmetric unit (Fig. 2, Fig. S4 and S5†). Powder X-ray diffraction (PXRD) patterns confirm the

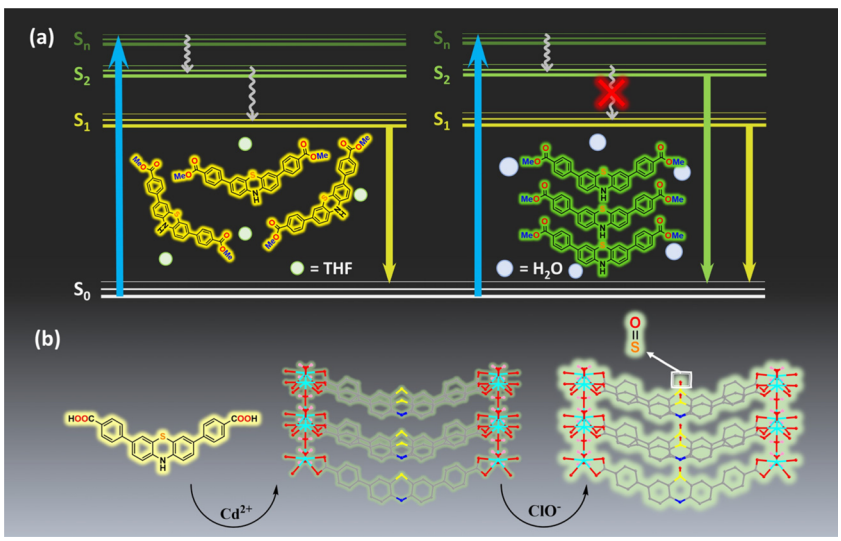

Scheme 1 (a) Different energy diagrams and relaxation paths of excited state **PTZ-dbo** in tetrahydrofuran (THF) and water. (b) Preparation of **Cd-PTZ-db** and the mechanism of the turn-on luminescence of **Cd-PTZ-db** in response to ClO^- (red spheres represent O atoms, and cyan spheres represent Cd atoms).

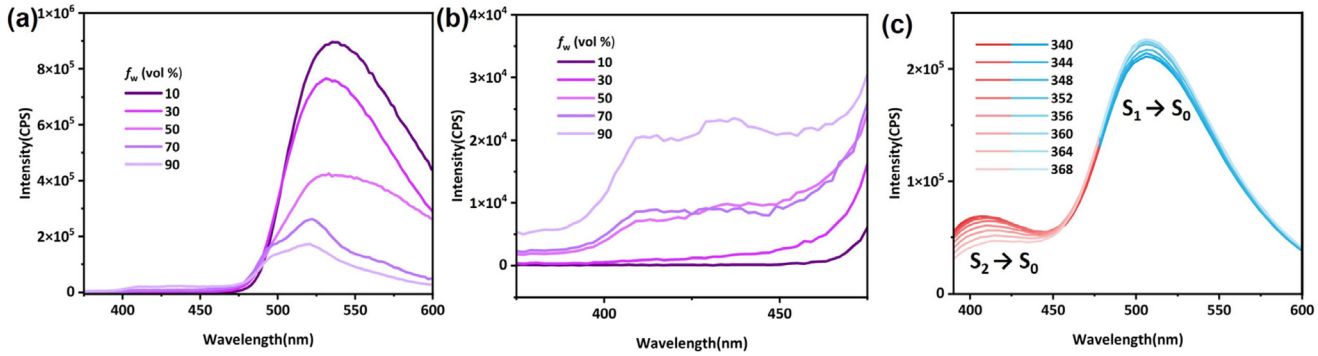

Fig. 1 (a) Photoluminescence (PL) spectra of **PTZ-dbo** in different solvents with 350 nm excitation; (b) a selected part of (a); (c) excitation-wavelength-dependent PL spectra of **PTZ-dbo** in water ($f_w = v_{water}/v_{THF+water}$, $C_{PTZ\text{-}dbo}$ = 1 μg mL^{-1}).

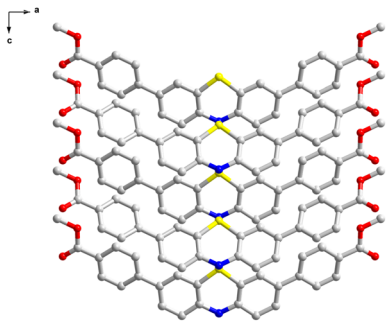

Fig. 2 2D structure of **PTZ-dbo** seen form *b*-axis (hydrogen atoms have been omitted for the sake of clarity).

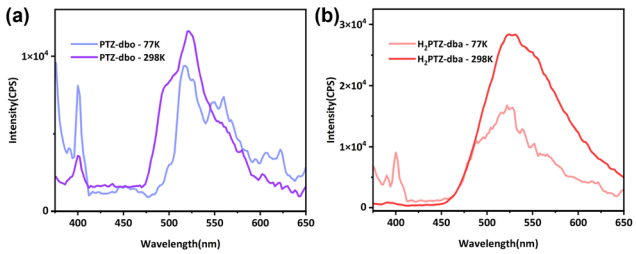

Fig. 3 (a) Solid PL spectra of **PTZ-dbo** at different temperatures; (b) solid PL spectra of H_2PTZ-dba at different temperatures.

structure consistency of the powder and crystal of **PTZ-dbo** (Fig. S6†). Furthermore, SCXRD demonstrates no obvious intermolecular interaction in the crystalline state as shown in Fig. S7.† The above results show that no intermolecular interactions or molecular changes occur when aggregated; therefore, intermolecular interactions and molecular changes are not responsible for multi-wavelength emissions.

These previous observations suggest that, such as AIE, these multi-wavelength emissions from the upper excited and lowest excited states, called anti-Kasha's rule emissions, may originate from RIM in the aggregate state.

Theoretically, intramolecular motion will also be restricted by low temperature, and the intensity of the upper excited state emission will be enhanced by lowering the temperature. On the basis of these considerations, temperature-dependent fluorescence spectra were recorded for **PTZ-dbo** and H_2PTZ-dba powders with the temperature at 77 K and 298 K, respectively. As shown in Fig. 3a, **PTZ-dbo** exhibited a 400 nm emission with 350 nm excitation, and its intensity tripled when the ambient temperature decreased from 298 to 77 K. However at 77 K, the emission at 525 nm decreased, indicating that RIM at low temperatures may alter the proportion of electron transitions from different excited states. The same phenomenon was also observed in H_2PTZ-dba (Fig. 3b). The increase was stronger compared to that of **PTZ-dbo**, possibly due to the greater impact of low temperature restriction, since H_2PTZ-dba is amorphous in the solid state. Moreover, the weak emission of H_2PTZ-dba at 400 nm indicates that the ordered structure, which can restrict the molecular motion, plays an important role in this short-wavelength emission.

Solid-state decay curves for two molecules were recorded at different temperatures (Fig. S8†). Their fluorescence lifetimes (τ) of the short-wavelength emission increased as the temperature decreased from 298 to 77 K. For instance, the τ of **PTZ-dbo** at 298 K was 7.17 ns, while at 77 K it increased to 8.08 ns. This indicates that the short-wavelength emission is dependent on the molecular mobility. The increases in τ and the relative strength of the short-wavelength emission with decreasing temperature show that restricting molecular motions is effective in achieving anti-Kasha's rule emission.

2.2 Anti-Kasha's rule emission mechanism

To comprehensively investigate the luminescence properties of the representative molecule **PTZ-dbo**, we preformed theoretical calculations to simulate the photophysical properties of **PTZ-dbo**, and the solid-state environment was taken into account by tuning the range-separation parameter ω.[30] The computational model was based on the single crystal structure of **PTZ-dbo**. Initially, the geometric structures of **PTZ-dbo** in the ground state (S_0) and lowest singlet excited state (S_1) were theoretically optimized in the solid phase at the LC-BLYP/def2-TZVP level. Calculated energy levels, electronic transition characters, and molecular orbitals for S_1 and S_2 in the crystals of **PTZ-dbo** are summarized in Fig. S9 and Table S1.† As

expected, there is a large difference in excitation energies (0.91 eV) between S_2 and S_1 for **PTZ-dbo**, which can greatly reduce the rate of IC between S_2 and S_1. Based on the optimized S_0 structure, the oscillator strength (f) for the electronic relaxation from S_1 to the ground state (S_0) was calculated to be 0.37970. A particularly surprising result is that S_2 has a much larger oscillator strength (f = 0.60280) than S_1, which is opposite to the common belief and does not obey Kasha's rule. These findings demonstrate that the emission of **PTZ-dbo** in the aggregate state is associated with the radiative transitions of S_2 and S_1. In other words, **PTZ-dbo** has anti-Kasha's rule behavior. This unusual anti-Kasha's rule emission may be caused by restriction of IC of high-level excited states to the lowest energy excited states when aggregated.

To verify the role that the restriction of the ordered structure plays in the anti-Kasha's rule emission, the investigation of intramolecular motion is further studied by femtosecond transient absorption (fs-TA).[31] As shown in Fig. 4a, and Fig. S10 and S11,† dilute solutions of H_2PTZ-dba and **PTZ-dbo** exhibit same absorption peaks at 578 nm under 355 nm excitation, reflecting their monomolecular properties. Measurements were also conducted in their solid film states for comparison. Fig. 4b shows the absorption peak of the H_2PTZ-dba film at 540 nm, and a time constant of 14.9 ps is determined when fitting the kinetics to a monoexponential function (Fig. 4c). This result coincides with the time of IC between excited states. In contrast, it can be seen that there is no absorption at 540 nm in the **PTZ-dbo** film (Fig. 4d), even though the absorption signal is largely obscured by its pronounced stimulated radiation. Since the film of H_2PTZ-dba is amorphous and **PTZ-dbo** can easily form a crystal structure in the aggregated state, their different excited state absorption indicates that it is RIM from the ordered structure in the aggregated state that restricts the IC process.

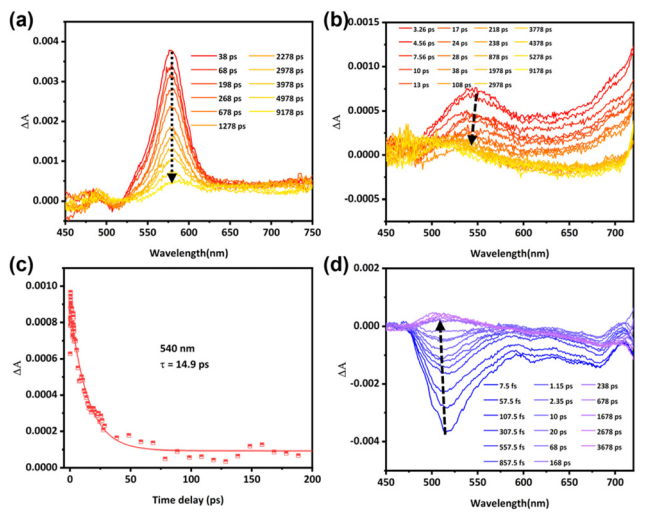

Fig. 4 (a) fs-TA spectra of H_2PTZ-dba in THF; (b) fs-TA spectra of H_2PTZ-dba in the film state; (c) kinetic traces of the H_2PTZ-dba film at 540 nm. The excitation wavelength is 355 nm. (d) fs-TA spectra of **PTZ-dbo** in the film state. Films were prepared by natural evaporation of their THF solution of 1 mM on a quartz substrate.

2.3 Crystal structure and stability of Cd-PTZ-db

As a material with chemical and structural tunability, MOFs can inherit the characteristics of organic ligands and rigid structure of the MOF can strengthen RIM through coordination.[10] To strengthen RIM, the **Cd-PTZ-db** complex was synthesized from H_2PTZ-dba and Cd^{2+} by a solvothermal method. **Cd-PTZ-db** successfully shares a similar structure and luminescence properties to those of **PTZ-dbo** (Fig. S12†), exhibiting multi-wavelength emission in the water suspension.

Cd-PTZ-db crystallizes in the orthorhombic space group $Pmc2_1$ and consists of half a Cd^{2+} ion and half a PTZ-dba^{2-} ligand in the asymmetric unit (Fig. S13†). Each Cd^{2+} ion is seven-coordinated by four carboxylate O atoms (O1, O2, O1A and O2A) from two different PTZ-dba^{2-} ligands and three O atoms (O3, O3A and O4) from coordinated water molecules. As shown in Fig. S14,† each PTZ-dba^{2-} ligand connects two Cd^{2+} ions, while each Cd^{2+} ion is linked by two PTZ-dba^{2-} ligands and three bridged water molecules. The adjacent layers are further connected by hydrogen bonds.

The thermal stability of **Cd-PTZ-db** was analyzed by thermogravimetric analysis (TGA). This result indicates that the decomposition temperature is up to 385 °C, revealing the good thermal stability of **Cd-PTZ-db** (Fig. S15†). The acidic and alkaline stability of **Cd-PTZ-db** is investigated in aqueous suspensions of pH = 1–14 for 2 days (Fig. S16†).

2.4 Response to hypochlorite (ClO^-)

ClO^- is widely used as a powerful oxidant in water treatment,[32] disinfection,[33] industrial manufacturing,[34,35] and other areas,[36] so precise control over ClO^- concentration in solvents is crucial. Additionally, ClO^- is a reactive oxygen species (ROS) and abnormal levels of it have been linked to diseases including atherosclerosis[37] and cancer.[38] Hence, the development of rapid and quantitative ClO^- detection methods bears immense significance for environmental and life sciences. Phenothiazine derivates are widely used in detecting ClO^- since the sulfur atom in phenothiazine can be oxidized by ClO^- into sulfoxide or sulfone. As shown in Fig. 5a and b, the short-wavelength emission of **PTZ-dbo** and H_2PTZ-dba disappears, and the 516 nm emission decreases after hypochlorite (ClO^-) stimulation, while the upper excited emission of **Cd-PTZ-db** is not only maintained but also increased after ClO^- stimulation, as shown in Fig. 5c. The short-wavelength emission of **Cd-PTZ-db** experiences a noteworthy increase as the concentration of ClO^- increases (Fig. 5d).

To demonstrate whether the fluorescence changes of **Cd-PTZ-db** were due to oxidation, some experiments were performed. The cyclic voltammograms indicated that **Cd-PTZ-db** can undergo oxidation (Fig S17†). Infrared Fourier transform (IRFT) spectroscopy (Fig. S18†) was employed to reveal the successful oxidation of **Cd-PTZ-db** through a 5 hours treatment with NaClO, and the appearance of the new peak at 963 cm^{-1} is evidence of the successful oxidation of sulfur to sulfoxide.

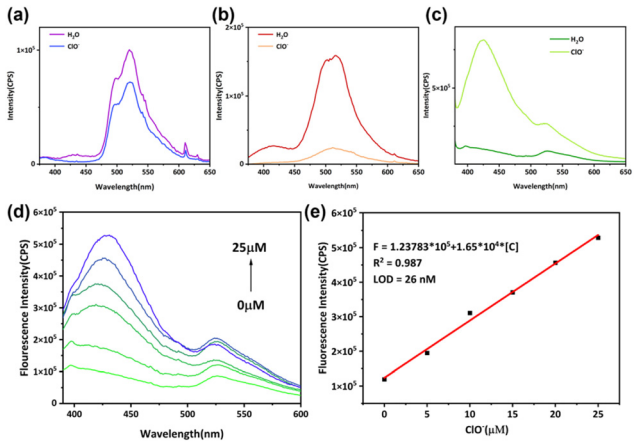

Fig. 5 PL spectra of **PTZ-dbo** (a), H_2PTZ-dba (b) and **Cd-PTZ-db** (c) in water before and after adding hypochlorite. (d) ClO^- dose-dependent luminescent spectra of complex **Cd-PTZ-db** suspensions under optimal sensing conditions and (e) the calibration curve for the detection of ClO^-.

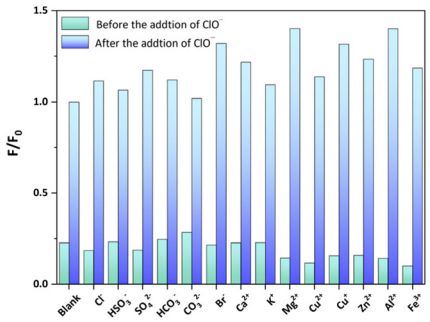

Fig. 6 Luminescence change of the complex **Cd-PTZ-db** suspension with interfering ions before and after mixing with 5 mM of NaClO.

High resolution mass spectroscopy (Fig. S19†) and X-ray photoelectron spectroscopy (Fig. S20†) also indicate the generation of sulfoxide.

The consistent PXRD patterns of **Cd-PTZ-db** (Fig. S21†) before and after the interaction with ClO^- confirm the stability of **Cd-PTZ-db**, and the observed turn-on luminescence effect is not due to disassociation. This stability is further corroborated by scanning electron microscopy (SEM) images (Fig. S22†). While traditional ClO^- probes based on phenothiazine derivatives mainly stem from intramolecular charge transfer, the simulated frontier molecular orbitals of H_2PTZ-dba do not reveal obvious changes following oxidation (Fig. S23†). Therefore, the turn-on luminescence response to ClO^- of **Cd-PTZ-db** in the short-wavelength emission range is attributed to the greater RIM from the increase of steric hindrance after oxidation in stable structures.

To verify the feasibility of **Cd-PTZ-db** for ClO^- detection, the luminescence intensity of the suspension was plotted against ClO^- concentration. Fig. 5e shows that there is a linear correlation between the luminescence intensity and ClO^- concentration in the range from 0 to 25 μM, which can be described as the fitting equation $F = 1.23783 \times 10^5 + 1.65 \times 10^4[C]$ ([C] represents the detected ClO^- concentration) with the correlation coefficient $R^2 = 0.987$. Meanwhile, the limit of detection (LOD) was calculated to be 26 nM (LOD = $3\delta/S$, δ: the standard deviation, and S: the slope of the fitted curve). Additionally, the sensing performance of **Cd-PTZ-db** was compared with previously reported luminescent probes designed for ClO^- detection (Table S2†). Impressively, **Cd-PTZ-db** stands out by providing a lower LOD. Therefore, **Cd-PTZ-db** can serve as a potential method for the detection of ClO^- in aqueous environments.

Sensing selectivity constitutes an important property of any sensing probe. As shown in Fig. 6, the selectivity of **Cd-PTZ-db** for ClO^- detection against other ions in deionized water was tested by subjecting the suspension of **Cd-PTZ-db** to individual mixtures with interfering ions, including Cl^-, HSO_3^-, SO_4^{2-}, HCO_3^-, CO_3^{2-}, Br^-, Ca^{2+}, K^+, Mg^{2+}, Cu^{2+}, Cu^+, Zn^{2+}, Al^{3+} and Fe^{3+}, and testing their luminescence performance. The results of these experiments show that the influence of the above ions on **Cd-PTZ-db** for the specific detection of ClO^- can be neglected, reaffirming its capability as an excellent probe for ClO^- detection.

The development of portable test paper strips for detection has gained significant attention due to their advantages in terms of rapid testing, cost-effectiveness, and user-friendliness. Herein, **Cd-PTZ-db**-coated paper strips were prepared. As evidenced by SEM images presented in Fig. S24a and S24b,† **Cd-PTZ-db** was successfully loaded onto the paper strips. The detection of ClO^- on the paper strips was performed using a spray bottle to gently spray ClO^- solution of different concentrations onto the paper strip. As shown in Fig. 7, the dry **Cd-PTZ-db**-coated paper strip exhibits the violet luminescence associated with the unaltered paper. When sprayed with deionized water under a 365 nm UV lamp, the luminescence diminishes. However, when sprayed with ClO^- solutions, the **Cd-PTZ-db**-coated paper strips emit a cyan light, and the luminescence intensity increases proportionally with the increase of ClO^- concentration. Impressively, these paper strips are capable of detecting ClO^- at concentrations as low as 10^{-6} M, meeting requirements set by the Food and Drug Administration for the residual ClO^- level in food after disinfection. Subsequent SEM images, obtained after the reaction, serve as conclusive evidence of the stability of **Cd-PTZ-db** within the paper strips (Fig. S24c and S24d†).

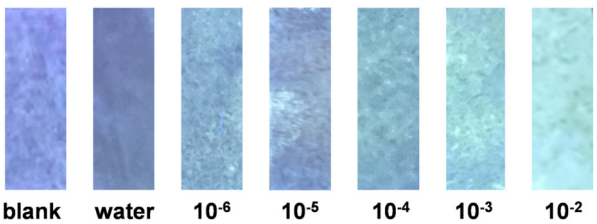

Fig. 7 Pictures of **Cd-PTZ-db**-coated paper strips (under a UV lamp of 365 nm) after spraying with different concentration (μM) NaClO solutions.

3. Conclusion

In summary, we have investigated the dual emissions of two phenothiazine derivatives, **PTZ-dbo** and H_2PTZ-dba, and a new 2D MOF, **Cd-PTZ-db**. The UV-vis absorption spectroscopy and SCXRD results demonstrate that their dual emissions do not come from intermolecular interactions or molecular changes. The observation of luminescence changes in the aggregated state following excitation wavelength and temperature changes are convincing evidence that the dual emissions emanate from the lowest and upper excited states, and these anti-Kasha's rule emissions are driven by RIM, which results from their aggregation arrangement. Calculations reveal the large energy gaps of **PTZ-dbo** in the rigid environment, the presence of which can be related to the suppression of IC of the upper excited state to the lowest energy excited state. Moreover, notable differences between the fs-TA spectra of H_2PTZ-dba and **PTZ-dbo** in solution and as films serve as evidence for the connection between the suppression of IC and the ordered structure. Moreover, **Cd-PTZ-db** withstands the oxidation of ClO^- and possesses remarkable selectivity and sensitivity for ClO^- detection in water with an impressive detection limit of 0.026 μM. An exciting development is the successful fabrication of portable ClO^- detection strips capable of detecting concentrations as low as 10^{-6} M. This achievement demonstrates the excellent selectivity, sensitivity, and stability of the **Cd-PTZ-db** sensor used for ClO^- detection, which has substantial practical utility. The results indicate that MOFs can not only possess the properties of organic ligands and metals but also inherit the structure of organic crystal arrangements and exhibit more stability. Thus, our research explores the relationship between anti-Kasha's rule emission and the restriction of intramolecular motion in the aggregated state and opens approaches for the design of other single-component, multi-emissive MOFs.

Author contributions

Tingting Wu planned and performed the experiments and prepared the original manuscript. Mingyuan Lei aided in the luminescence experiments and was involved in writing the manuscript. Fayuan Ge aided in the crystal analysis and thermogravimetric experiments and participated in revising the manuscript. Yang Liu aided in writing and revising the manuscript. Minqi Xia planned and performed the theoretical calculations. Lijun Yang guided the theoretical calculations and provided the software support. Hegen Zheng guided writing review and editing and was responsible for the funding acquisition and project supervision. All the authors contributed to scientific discussions.

Conflicts of interest

The authors declare no conflicts of interest.

Acknowledgements

The authors acknowledge the support of the National Natural Science Foundation of China (21771101). We acknowledge Prof. Zhiqiang Shi (School of Chemistry and Chemical Engineering, Suzhou University, Suzhou) for calculation support. We are grateful to Prof. Chunfeng Zhang and San Zhang (National Laboratory of Solid State Microstructures, School of Physics and Collaborative Innovation Center for Advanced Microstructures, Nanjing University, Nanjing) for femtosecond transient absorption (fs-TA) spectroscopy support.

References

1 M. Kasha and S. P. McGlynn, Molecular electronic spectroscopy, *Annu. Rev. Phys. Chem.*, 1956, **7**, 403–424.
2 A. Blice-Baum, A. Van Dyke, I. Sigmon, E. A. Salter, A. Wierzbicki, Y. Pocker and G. T. Spyridis, Computational and spectroscopic studies concerning the solvatochromic behavior of 1,3-disubstituted azulenes, *Int. J. Quantum Chem.*, 2006, **106**, 2331–2338.
3 Y. Y. Zhou, Y. P. Zhuang, X. Li, H. Ågren, L. Yu, J. D. Ding and L. L. Zhu, Selective dual-channel imaging on cyanostyryl-modified azulene systems with unimolecularly tunable visible-near infrared luminescence, *Chem. Eng. J.*, 2017, **23**, 7642–7647.
4 Y. Y. Zhou, Q. Zou, J. Qiu, L. J. Wang and L. L. Zhu, Rational design of a green-light-mediated unimolecular platform for fast switchable acidic sensing, *J. Phys. Chem. Lett.*, 2018, **9**, 550–556.
5 Q.-S. Zhang, S.-C. Wang, X.-H. Xiong, P.-Y. Fu, X.-D. Zhang, Y.-N. Fan and M. Pan, High-temperature and dynamic RGB (Red-Green-Blue) long-persistent luminescence in an anti-Kasha organic compound, *Angew. Chem., Int. Ed.*, 2022, **61**, e202205556.
6 H. Sun, S.-S. Sun, F.-F. Han, Y. Zhao, M.-D. Li, B.-X. Miao, J. Nie, R. Zhang and Z.-H. Ni, Water-stimuli-responsive dynamic fluorescent switch from Kasha's rule to anti-Kasha's rule based on a tetraphenylethene substituted Schiff base, *Chem. Eng. J.*, 2021, **405**, 127000.
7 Y. B. Xie, L. Y. Liu, Z. T. Huang, H. X. Miao, W. J. Zhaxi, F. N. Duan, W. Huang and D. Y. Wu, Multicomponent anti-Kasha's rule emission from nanotubular metal–organic frameworks for selective detection of small molecules, *Inorg. Chem.*, 2023, **62**, 3170–3177.
8 J. Guo, J. Fan, L. Lin, J. Zeng, H. Liu, C.-K. Wang, Z. Zhao and B. Z. Tang, Mechanical insights into aggregation-induced delayed fluorescence materials with anti-Kasha behavior, *Adv. Sci.*, 2019, **6**, 1801629.
9 Y.-H. Wu, H. Xiao, B. Chen, R. G. Weiss, Y.-Z. Chen, C.-H. Tung and L.-Z. Wu, Multiple-state emissions from neat, single-component molecular solids: suppression of Kasha's rule, *Angew. Chem., Int. Ed.*, 2020, **59**, 10173–10178.

10 H.-Q. Yin, X.-Y. Wang and X.-B. Yin, Rotation restricted emission and antenna effect in single metal–organic frameworks, *J. Am. Chem. Soc.*, 2019, **141**, 15166–15173.
11 N. B. Shustova, A. F. Cozzolino and M. Dinca, Conformational locking by design: relating strain energy with luminescence and stability in rigid metal-organic frameworks, *J. Am. Chem. Soc.*, 2012, **134**, 19596–19599.
12 N. B. Shustova, A. F. Cozzolino, S. Reineke, M. Baldo and M. Dincă, Selective turn-on ammonia sensing enabled by high-temperature fluorescence in metal–organic frameworks with open metal sites, *J. Am. Chem. Soc.*, 2013, **135**, 13326–13329.
13 X. J. Gao and H. G. Zheng, The difference in the CO_2 adsorption capacities of different functionalized pillar-layered metal–organic frameworks (MOFs), *Dalton Trans.*, 2021, **50**, 9310–9316.
14 Q. Yan, X. D. Duan, Y. Liu, F. Y. Ge and H. G. Zheng, A hybridization cage-confinement pyrolysis strategy for ultra-small Ni_3Fe alloy coated with N-doped carbon nanotubes as bifunctional oxygen electrocatalysts for Zn–air batteries, *J. Mater. Chem. A*, 2023, **11**, 1430–1438.
15 X. D. Duan, M. Q. Xia, X. X. Hu, L. J. Yang and H. G. Zheng, Interfacing MnO and FeCo alloy inside N-doped carbon hierarchical porous nanospheres derived from metal–organic framework to boost high-performance oxygen reduction for Zn–air batteries, *Nanoscale*, 2022, **14**, 16516–16523.
16 Y. M. Zhang, S. Yuan, G. Day, X. Wang, X. Y. Yang and H. C. Zhou, Luminescent sensors based on metal-organic frameworks, *Coord. Chem. Rev.*, 2018, **354**, 28–45.
17 M. Lei, F. Ge, S. Ren, X. Gao and H. Zheng, A water-stable Cd-MOF and corresponding MOF@melamine foam composite for detection and removal of antibiotics, explosives, and anions, *Sep. Purif. Technol.*, 2022, **286**, 120433.
18 M. Oggianu, V. Mameli, M. A. Hernández-Rodríguez, N. Monni, M. Souto, C. D. S. Brites, C. Cannas, F. Manna, F. Quochi, E. Cadoni, N. Masciocchi, A. N. C. Neto, L. D. Carlos and M. L. Mercuri, Insights into NdIII to YbIII Energy Transfer and Its Implications in Luminescence Thermometry, *Chem. Mater.*, 2024, **36**, 3452–3463.
19 Y. Y. Lu, W. W. Zhan, Y. He, Y. T. Wang, X. J. Kong, Q. Kuang, Z. X. Xie and L. S. Zheng, MOF-templated synthesis of porous Co_3O_4 concave nanocubes with high specific surface area and their gas sensing properties, *ACS Appl. Mater. Interfaces*, 2014, **6**, 4186–4195.
20 V. J. Witherspoon, L. M. Yu, S. Jawahery, E. Braun, S. M. Moosavi, S. K. Schnell, B. Smit and J. A. Reimer, Translational and rotational motion of C8 aromatics adsorbed in isotropic porous media (MOF-5): NMR studies and MD simulations, *J. Phys. Chem. C*, 2017, **121**, 15456–15462.
21 J. Perego, C. X. Bezuidenhout, I. Villa, F. Cova, R. Crapanzano, I. Frank, F. Pagano, N. Kratochwill, E. Auffray, S. Bracco, A. Vedda, C. Dujardin, P. E. Sozzani, F. Meinardi, A. Comotti and A. Monguzzi, Highly luminescent scintillating hetero-ligand MOF nanocrystals with engineered Stokes shift for photonic applications, *Nat. Commun.*, 2022, **13**, 3504.
22 G. Valente, M. Esteve-Rochina, S. P. C. Alves, J. M. G. Martinho, E. Ortí, J. Calbo, F. A. A. Paz, J. Rocha and M. Souto, Perylene-Based Coordination Polymers: Synthesis, Fluorescent J-Aggregates, and Electrochemical Properties, *Inorg. Chem.*, 2023, **62**, 7834–7842.
23 F. M. A. Noa, E. S. Grape, M. Åhlén, W. E. Reinholdsson, C. R. Göb, F. X. Coudert, O. Cheung, A. K. Inge and L. Öhrström, Chiral lanthanum metal–organic framework with gated CO_2 sorption and concerted framework flexibility, *J. Am. Chem. Soc.*, 2022, **144**, 8725–8733.
24 M. Nakagawa, S. Kusaka, A. Kiyose, T. Nakajo, H. Iguchi, M. Mizuno and R. Matsuda, Beyond the conventional limitation of photocycloaddition reaction in the roomy nanospace of a metal–organic framework, *J. Am. Chem. Soc.*, 2023, **145**, 12059–12065.
25 F. Y. Ge, G. H. Sun, L. Meng, S. S. Ren and H. G. Zheng, Four new luminescent metal–organic frameworks as multifunctional sensors for detecting Fe^{3+}, $Cr_2O_7^{2-}$ and nitromethane, *Cryst. Growth Des.*, 2020, **20**, 1898–1904.
26 X. J. Gao, G. H. Sun, F. Y. Ge and H. G. Zheng, Three anionic indium–organic frameworks for highly efficient and selective dye adsorption, lanthanide adsorption, and luminescence regulation, *Inorg. Chem.*, 2019, **58**, 8396–8407.
27 Z. Z. Lu, R. Zhang, Y. Z. Li, Z. J. Guo and H. G. Zheng, Solvatochromic behavior of a nanotubular metal—organic framework for sensing small molecules, *J. Am. Chem. Soc.*, 2011, **133**, 4172–4174.
28 W. Yan, C. L. Zhang, S. G. Chen, L. J. Han and H. G. Zheng, Two lanthanide metal–organic frameworks as remarkably selective and sensitive bifunctional luminescence sensor for metal ions and small organic molecules, *ACS Appl. Mater. Interfaces*, 2017, **9**, 1629–1634.
29 D. M. Chen, N. N. Zhang, C. S. Liu and M. Du, Template-directed synthesis of a luminescent Tb-MOF material for highly selective Fe^{3+} and Al^{3+} ion detection and VOC vapor sensing, *J. Mater. Chem. C*, 2017, **5**, 2311–2317.
30 H. T. Sun, Z. B. Hu, C. Zhong, X. K. Chen, Z. R. Sun and J.-L. Brédas, Impact of dielectric constant on the singlet–triplet gap in thermally activated delayed fluorescence materials, *J. Phys. Chem. Lett.*, 2017, **8**, 2393–2398.
31 H. K. Zhang, L. L. Du, L. Wang, J. K. Liu, Q. Wan, R. T. K. Kwok, J. W. Y. Lam, D. L. Phillips and B. Z. Tang, Visualization and manipulation of molecular motion in the solid state through photoinduced clusteroluminescence, *Phys. Chem. Lett.*, 2019, **10**, 7077–7085.
32 F. G. Meng, S. Q. Zhang, Y. Oh, Z. B. Zhou, H. S. Shin and S. R. Chae, Fouling in membrane bioreactors: an updated review, *Water Res.*, 2017, **114**, 151–180.
33 G. Kampf, D. Todt, S. Pfaender and E. Steinmann, Persistence of coronaviruses on inanimate surfaces and their inactivation with biocidal agents, *J. Hosp. Infect.*, 2020, **104**, 246–251.

34 B. Jung, J. K. Yoon, B. Kim and H. W. Rhee, Effect of molecular weight of polymeric additives on formation, permeation properties and hypochlorite treatment of asymmetric polyacrylonitrile membranes, *J. Membr. Sci.*, 2004, **243**, 45–57.
35 K. M. Macounová, N. Simic, E. Ahlberg and P. Krtil, Electrochemical water-splitting based on hypochlorite oxidation, *J. Am. Chem. Soc.*, 2015, **137**, 7262–4265.
36 W. A. Rutala and D. J. Weber, Clin. Uses of inorganic hypochlorite (bleach) in health-care facilities, *Microbiol. Rev.*, 1997, 597–610.
37 D. I. Pattison, C. L. Hawkins and M. J. Davies, Hypochlorous acid-mediated oxidation of lipid components and antioxidants present in low-density lipoproteins: absolute rate constants, product analysis, and computational modeling, *Chem. Res. Toxicol.*, 2003, **16**, 439–449.
38 B. Pan, H. Ren, X. F. Lv, Y. Y. Zhao, B. Q. Yu, Y. B. He, Y. J. Ma, C. G. Niu, J. G. Kong, F. Z. Yu, W. B. Sun, Y. Y. Zhang, B. Willard and L. M. Zheng, Hypochlorite-induced oxidative stress elevates the capability of HDL in promoting breast cancer metastasis, *J. Transl. Med.*, 2012, **10**, 65.